DOI: 10.1002/ejic.201000963

Homo- and Heterometallic Terbium Alkoxides – Synthesis, Characterization and Conversion to Luminescent Oxide Nanostructures

Eva Hemmer,[a] Volker Huch,[b] Matthias Adlung,[c] Claudia Wickleder,[c] and Sanjay Mathur*[d]

Keywords: Lanthanides / Terbium / Aluminium / Alkoxides / Nanostructures / Luminescence / Sol-gel process / Optical materials

Terbium alkoxides in homometallic – $[Tb_3(\mu_3\text{-}OtBu)_2(\mu_2\text{-}OtBu)_3(OtBu)_4(HOtBu)_2]$ (**1**), $[Tb\{OC(tBu)_3\}_3(THF)]$ (**2**) – and heterometallic configurations – $[TbAl(\mu_2\text{-}OiPr)_3(OiPr)_3(iPrOH)]_2$ (**3**), $[TbAl_3(\mu_2\text{-}OiPr)_6(OiPr)_6]$ (**4**) – were synthesized and characterized by single-crystal X-ray diffraction. Decomposition of **1** and **2** under solvothermal conditions produced $Tb(OH)_3$ nanorods, whereby the material formation and crystallization were influenced by the steric profile of the organic ligand, which controlled the hydrolysis and condensation reactions of the precursor molecules. Monophasic terbium aluminate in the perovskite phase ($TbAlO_3$) was obtained by the sol–gel processing of **3**. Heterometallic frameworks present in **3** and **4** were, however, unstable under solvothermal conditions and resulted in hydroxide–oxide composites $[Tb(OH)_3/Al_2O_3/Al(OH)_3]$. Compound **4** exhibited sufficient vapour pressure to be used in the chemical vapour deposition (CVD) process to grow Tb–O–Al thin films. Crystalline compositions obtained on $MgAl_2O_4$ and SiO_2 (quartz) substrates were garnet and perovskite phases, and were ascribed to the crystallographic relationship between the substrate and CVD deposits. The optical properties of the powders obtained were studied by photoluminescence spectroscopy.

Introduction

Trivalent lanthanide alkoxides favour a trinuclear framework, particularly when *tert*-butoxy groups are chosen as ligands, resulting in molecular compounds of general formula $[Ln_3(OtBu)_9(HOtBu)_2]$, in which two neutral alcohol molecules are coordinated to the Ln^{III} centres (Scheme 1).[1] Formation of a crystalline Pr^{III} *tert*-butoxide was described by Hubert-Pfalzgraf et al.; however, no crystallographic data on the molecular structure was reported.[2] We have recently characterized the praseodymium and gadolinium *tert*-butoxides,[3] which were found to be analogous to the yttrium,[4] lanthanum,[1] cerium,[5] erbium[6] and dysprosium[7] compounds.

Herein we report new terbium-containing single- and mixed-metal alkoxides, and their application in the preparation of terbium-based ceramics by solvothermal, sol–gel and chemical vapour deposition techniques. Metal alkoxides are attractive precursors to metal oxides due to the presence of pre-existing metal–oxygen units, which facilitate the formation of nanocrystalline oxide materials at low temperatures (<1000 °C).[8] Their high solubility and/or volatility, which can be tuned by the electronic and steric factors, allows easy purification by sublimation or recrystallisation.[9] A further advantage of these preparations of pure metal–oxide ceramics is the absence of other elements such as Cl, which may be introduced in the crystalline framework when precursors such as metal halides are used. Although the synthesis of binary oxides from monometallic alkoxides $[M(OR)_x \rightarrow MO_x]$ appears straightforward, formation of single phase mixed-cation ceramics (e.g., $LiNbO_3$, Co-

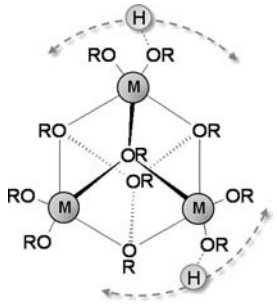

Scheme 1. General molecular structure of $[Ln_3(OtBu)_9(HOtBu)_2]$ (the dotted lines to ROH groups represent the delocalization of the alcohol molecules rotating around the Ln^{III} centres).

[a] Department of Materials Science and Technology, Tokyo University of Science,
2641 Yamazaki, 278-8510 Chiba, Japan
[b] Institute of Inorganic Chemistry, Saarland University, Building C4 1,
66123 Saarbruecken, Germany
[c] Institute of Inorganic Chemistry, University of Siegen,
Adolf-Reichwein-Str., 57068 Siegen, Germany
[d] Institute of Inorganic Chemistry, University of Cologne,
Greinstr. 6, 50939 Cologne, Germany
Fax: +49-221-470-5899
E-mail: sanjay.mathur@uni-koeln.de
Supporting information for this article is available on the WWW under http://dx.doi.org/10.1002/ejic.201000963.

Fe_2O_4, $BaZrO_3$) from a mixture of component alkoxides is not obvious due to the differential Lewis acidity and basicity of individual metal alkoxides. Consequently, besides the major phase, minor phase separation or element segregation is generally observed in mixed-cation ceramics. The fact that the redistribution of elements is thermodynamically favoured and cannot be suppressed in a simple mixture of constituent metal–organic derivatives limits the predictability of the final phase (composition) of precursor-based routes. Nevertheless, heterometal alkoxides enable the formation of homogenates, in which the phase-forming elements are bound chemically to each other. Preserving the elemental network given in the alkoxide precursor enables its transformation into ceramics with a controlled mixed-metal matrix. We have demonstrated the potential of molecular precursors in the preparation of single phase mixed-metal oxides with different chemical compositions such as AB_2O_4,[10] ABO_3[11] and $A_3B_5O_{12}$[4,12] (A = Co, Ni, Cu, Mg, Ba, Gd, Y; B = Al, Ti, Zr, Fe).

Besides nanoparticles (zero-dimensional) and thin films (two-dimensional), one-dimensional structures as nanorods, nanotubes and nanowires are gaining increasing attention. The preparation of highly luminescent $Tb(OH)_3@SiO_2$ nanotubes by soft-template synthesis was described by Huong et al.,[13] and the synthesis of $Eu(OH)_3$ nanorods by microwave irridation for biomedical applications was reported by Patra et al.[14] Due to the crystallisation of lanthanide hydroxide in the hexagonal lattice, $Ln(OH)_3$ nanorods can also be grown by template-free solvothermal synthesis and be easily transformed into anisotropic Ln_2O_3 nanostructures, which are promising for optical applications.[15] Herein, the main advantage of the solvothermal process is the synthesis of crystalline and isolated fine structures at low temperatures, whereas most wet-chemical approaches require subsequent heat treatment for crystallization inducing the risk of agglomerations by the sintering effect.[16] Due to the intense emission of Tb^{3+} ions near 544 nm, terbium-containing materials find applications as green emitting phosphors[17] in luminescent materials (Ce^{3+},Tb^{3+}:$LaPO_4$, Tb^{3+}:$CePO_4$, Eu^{3+}/Tb^{3+}:SrB_4O_7),[18] display applications (Tb^{3+}:YAG)[19] and as highly photostable biomolecule markers (Tb^{3+}:Gd_2O_3).[20] Phase separation is crucial for doped systems, where the functional behaviour of the material depends on the chemical homogeneity of the phase and an optimal distribution of the dopant ions.

The aim of this study is to develop new Tb-containing molecular compounds and investigate their precursor chemistry in solvothermal, sol–gel and CVD[21] processes.

Results and Discussion

Precursor Synthesis

Terbium *tert*-butoxide was prepared by the alcoholysis of terbium hexamethyldisilylamide [Tb{N(SiMe$_3$)$_2$}$_3$] with an excess of *tert*-butyl alcohol.[1] Colourless crystals obtained from a mixture of hexane and THF at –20 °C were identified as [Tb_3(O*t*Bu)$_9$(HO*t*Bu)$_2$] (**1**) by X-ray structure analysis. Compound **1** crystallizes in the monoclinic space group $P2_1/c$ and is isotypical with the analogous yttrium and lanthanum derivatives.[1,4] The molecular structure of **1** (Figure 1) contains three terbium atoms building a triangular framework supported by two doubly-bridging alkoxy ligands along the sides of the triangle (O3, O4 and O5). Two additional μ_3-bridging alkoxy ligands (O1 and O2) are present below and above the triangular plane, stretched by the three Tb atoms, resulting in sixfold oxygen coordination and a distorted octahedral geometry around the Tb centres.[22] One of the terbium atoms (Tb1) bears two alkoxy ligands, whereas Tb2 and Tb3 are each coordinated by an alkoxy group and a *tert*-butyl alcohol ligand. This structural inhomogeneity is reflected in the corresponding bond angles; the presence of a hydrogen bond [RO···HO(R)Tb] between anionic (OR^-) and protonated (ROH) ligands is indicated by comparing the O8–Tb2–O9 and O10–Tb3–O11 angles with the much smaller O6–Tb2–O7 angle (Table 1).

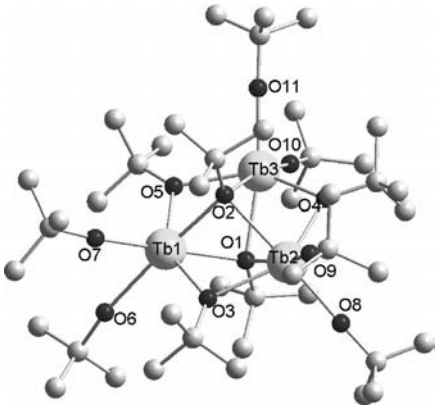

Figure 1. Molecular structure of [Tb_3(O*t*Bu)$_9$(HO*t*Bu)$_2$] (**1**) (hydrogen atoms are omitted for clarity).

Table 1. Selected bond lengths and angles of [Tb_3(O*t*Bu)$_9$(HO*t*Bu)$_2$] (**1**).

Bond lengths [Å]		Angles [°]	
Tb1–O1	2.403(3)	O6–Tb1–O7	72.29(14)
Tb1–O2	2.343(3)	O8–Tb2–O9	89.1(2)
Tb1–O3	2.285(4)	O10–Tb3–O11	84.2(2)
Tb1–O5	2.320(4)	Tb1–O3–Tb2	98.35(14)
Tb1–O6	2.609(4)	Tb1–O5–Tb3	97.84(14)
Tb1–O7	2.114(4)	Tb2–O4–Tb3	101.11(13)

The profound influence of the steric profile of the alkoxy ligand on the nuclearity of the molecule and the coordination sphere of the central metal atom was observed when the *tert*-butoxy groups were replaced by bulkier tris-*tert*-butoxy (tritox) ligands (Scheme 2).

Reaction of [Ln{N(SiMe$_3$)$_2$}$_3$] (Ln = Nd, Ce) with three equivalents of HOC(*t*Bu)$_3$ resulted in [Ln(tritox)$_3$(THF)] as shown by NMR spectroscopy.[23,24] Formation of solvent-free holmium tritox was confirmed by IR spectroscopy, although synthesis of the homoleptic dysprosium tritox failed.[25] Furthermore, the reaction between [Ln{N-

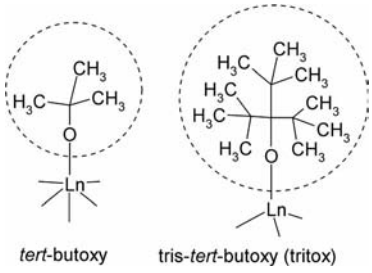

Scheme 2. Steric profiles of the *tert*-butoxy and tris-*tert*-butoxy (tritox) ligand.

$(SiHMe_2)_2\}_3]$ and $HOC(tBu)_3$ resulting in the homoleptic complexes $Ln(tritox)_3$ (Ln = Y, Nd), as well as structurally similar compounds $Ln(OR)_3$ with aryl ligands have been reported.[26] We show here that the reaction of $[Tb\{N(SiMe_3)_2\}_3]$ with $HOC(tBu)_3$ in THF produces monomeric $[Tb\{OC(tBu)_3\}_3(THF)]$ (**2**) with a pseudotetrahedral coordination of the terbium atom constituted by three tritox ligands and one coordinated THF molecule (recrystallisation was performed in an n-hexane/THF mixture) (Figure 2). Attempts to obtain a THF-free compound were not successful.

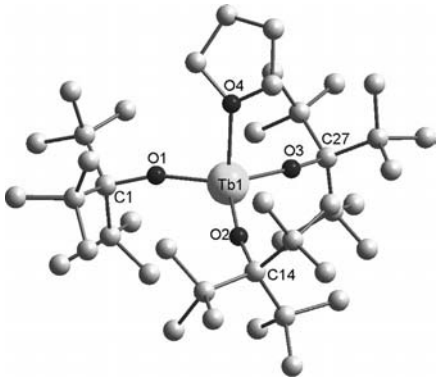

Figure 2. Molecular structure of $[Tb\{OC(tBu)_3\}_3(THF)]$ (**2**) (hydrogen atoms are omitted for clarity).

The strong steric repulsion between the tritox ligands leads to increased bond angles [O1–Tb1–O2 119.33(18)°, O2–Tb1–O3 116.50(18)°, O1–Tb1–O3 116.98(19)°] compared to the *tert*-butoxide derivative (Table 2). Angles between the coordinated THF molecule and the tritox ligands [O4–Tb1–O1 98.96(18)°, O4–Tb1–O2 102.06(18)°, O4–Tb1–O3 95.85(19)°] are smaller than expected for tetrahedral angles (109.5°) resulting in a distorted trigonal pyramidal molecular geometry. The Tb–O bond lengths in the mononuclear **2** are shorter (average bond length 2.185 Å) than those found in **1** (average bond length 2.343 Å), which shows the interplay of electronic and structural factors. The electron donating power of *tert*-butyl groups (basicity) decreases with increasing coordination of alkoxy oxygen atoms to the metal centre (terminal < μ_2-bridging < μ_3-bridging). Due to the fact that **2** contains only terminal alkoxy groups, the Tb–O distances are shorter (terminal alkoxy groups O1–O3 2.113 Å) compared to those of **1** (terminal alkoxy groups O6–O11 2.254 Å, μ_2-bridging O3–O5: 2.332 Å, μ_3-bridging O1–O2 2.443 Å).

Table 2. Selected bond lengths and angles of $[Tb\{OC(tBu)_3\}_3(THF)]$ (**2**).

Selected Distances [Å]		Selected Angles [°]	
Tb1–O1	2.111(4)	O1–Tb1–O2	119.33(18)
Tb1–O2	2.121(4)	O1–Tb1–O3	116.98(19)
Tb1–O3	2.107(4)	O2–Tb1–O3	116.50(18)
Tb1–O4	2.401(5)	O1–Tb1–O4	98.96(18)

Lanthanide-containing heterometallic alkoxides have been prepared by (i) condensation reactions between constituent alkoxides and (ii) salt elimination reactions between $LnCl_3$ and $KAl(OiPr)_4$[27] as described by Mehrotra et al.[28] In addition, heterometallic alkoxides with Ln = Y, Pr, Nd, Gd, Er and Yb and M = Fe or Al have been prepared by ligand exchange reactions between Ln and M-*tert*-butoxides with excess 2-propanol.[29] Samarium aluminium alkoxides have been obtained by the reaction of samarium amide and aluminium alkoxide with excess isopropanol.[30] The heterometallic Tb–Al compound $[TbAl(OiPr)_6(iPrOH)]_2$, with a Tb:Al ratio of 1:1, was obtained by the equimolar reaction of **1** and aluminium isopropoxide in an $iPrOH/C_6H_6$ mixture. A concentrated solution produced $[TbAl(OiPr)_6(iPrOH)]_2$ (**3**) as colourless crystals, which was shown by single crystal diffraction to be a centrosymmetric dimer (Figure 3) with an inversion centre lying in the middle of the central Tb_2O_2 ring [Tb1–O1: 2.2768(14) Å, Tb1–O1#1: 2.2868(14) Å], whereby the Tb^{3+} ions form the centre of a distorted tetragonal bipyramid.

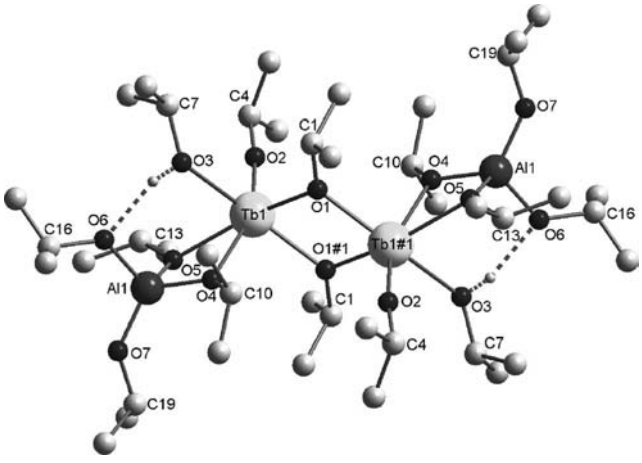

Figure 3. Molecular structure of $[TbAl(OiPr)_6(iPrOH)]_2$ (**3**) (hydrogen atoms are omitted for clarity).

The three μ_2-bridging oxygen atoms O1, O4 and O5, and O2 of the terminal alkoxy ligand form the equatorial plane around the central terbium cation [O1–Tb1–O2: 105.95(7)°, O2–Tb1–O5: 95.51(6)°, O4–Tb1–O5: 63.43(5)°, O1–Tb1–O4: 94.07(5)°]. In an ionic formalism, the overall structure can be described as the fusion of two tetrahedral $[Al(OiPr)_4]^-$ units to a central $[(ROH)(OR)Tb(\mu_2\text{-}OiPr)_2Tb(OR)(ROH)]^{2+}$ unit.[31] The Al–O bond lengths are shorter

than the Tb–O bonds [Al1–O4: 1.7707(15) Å, Al1–O5: 1.7856(14) Å, vs. Tb1–O4: 2.3861(13) Å, Tb1–O5: 2.3955(15) Å] demonstrating a better overlap of the Al and O orbitals due to similar van der Waals radii (Table 3).

Table 3. Selected bond lengths and angles of $[TbAl(OiPr)_6(iPrOH)]_2$ (**3**).

Bond lengths [Å]		Angles [°]	
Tb1–O1	2.2768(14)	O1#1–Tb1–O3	160.86(5)
Tb1–O1#	2.2801(16)	O1–Tb1–O2	105.95(7)
Tb1–O2	2.0681 (15)	O1–Tb1–O3	92.83(6)
Tb1–O3	2.4478(18)	O1–Tb1–O4	94.07(5)
Tb1–O4	2.3861(13)	O4–Al1–O5	89.95(7)
Tb1–O5	2.3955(15)	O6–Al1–O7	111.37(8)
Al1–O4	1.7707(15)		
Al1–O5	1.7856(14)		
Al1–O6	1.7422(17)		
Al1–O7	1.7005(16)		

The reaction of terbium *tert*-butoxide and aluminium isopropoxide in a 1:3 molar ratio produced $[Tb\{Al(OiPr)_4\}_3]$ (**4**). This compound can also be prepared by a salt elimination reaction between $TbCl_3$ and three equivalents of $KAl(OiPr)_4$.[27a] X-ray structural analysis revealed a monomer with a central Tb^{3+} ion surrounded by three $[Al(OiPr)_4]$ units resulting in a sixfold coordination around the Tb centres (Figure 4).

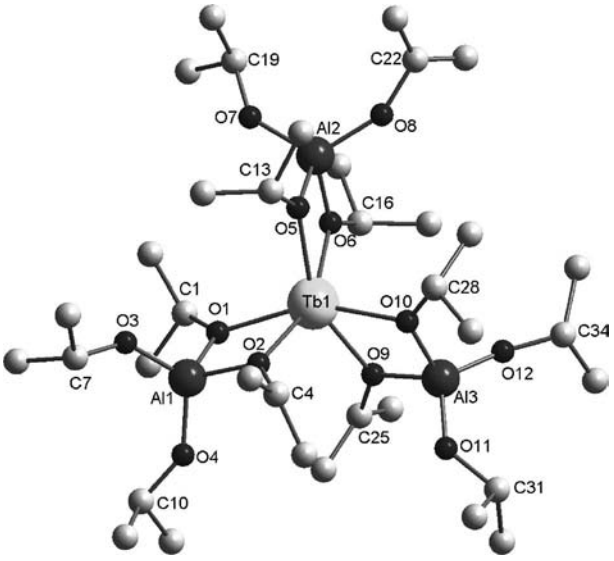

Figure 4. Molecular structure of $[Tb\{Al(OiPr)_4\}_3]$ (**4**) (hydrogen atoms are omitted for clarity).

The structural motif was originally proposed by Mehrotra[28] and was also reported for aluminium lanthanide alkoxides-containing ligands other than O*t*Bu and O*i*Pr.[32] The bond lengths (Table 4) of the central Tb atom and the μ_2-bridging oxygen atoms in **4** [2.281(4) Å (Tb1–O9) to 2.302(4) Å (Tb1–O6)] correlate well with praseodymium and erbium derivatives.[12b,27a,27b] The Al–O bond lengths [1.684(6) Å (Al1–O3) to 1.815(5) Å (Al2–O5)] and bond angles in **4** are comparable to these found in analogous Ln–Al compounds. In contrast to Pr and Nd alkoxy aluminates[12b] the Tb–Al compound crystallizes without any coordinated alcohol molecules. Similar alcohol-free structures have been observed for Er–Al[27a] and Eu–Al[27c] derivatives.

Table 4. Selected bond lengths and angles of $[Tb\{Al(OiPr)_4\}_3]$ (**4**).

Bond lengths [Å]		Angles [°]	
Tb1–O1	2.292(5)	O1–Tb1–O2	66.17(15)
Tb1–O2	2.292(4)	O1–Al1–O2	87.7(2)
Al1–O1	1.809(5)	O3–Al1–O4	118.8(3)
Al1–O2	1.802(5)		
Al1–O3	1.684(6)		
Al1–O4	1.696(6)		

Optical Properties of Compound 1

In order to analyse the optical properties of terbium alkoxides, **1** was chosen for investigation by photoluminescence spectroscopy. Figure 5 shows the excitation and emission spectra of **1** obtained at 10 K. Under UV excitation the characteristic Tb^{3+} emission peaks are detected with a maximum at 543 nm, which can be attributed to the $^5D_4 \rightarrow {}^7F_5$ transition. Further peaks observed at 495, 591, 623 and 656 nm are assigned, based on previous investigations, to the $^5D_4 \rightarrow {}^7F_6$, $^5D_4 \rightarrow {}^7F_4$, $^5D_4 \rightarrow {}^7F_3$ and $^5D_4 \rightarrow {}^7F_2$ transitions, respectively.[33]

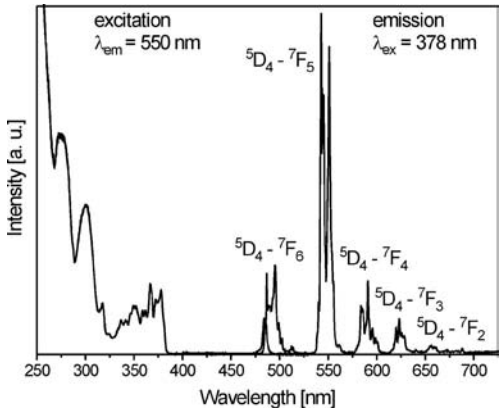

Figure 5. Photoluminescence spectra of **1** at T = 10 K.

Material Synthesis and Characterization

Terbium Hydroxide Nanostructures by Solvothermal Synthesis

The decomposition of suitable precursor molecules under basic conditions favours the formation of crystalline elongated lanthanide hydroxide, $Ln(OH)_3$, structures in particular for lighter rare earth elements.[34] Decomposition behaviour of **1** and **3** was further investigated by thermogravimetric analysis and thermogravimetric differential thermal analysis (TG-DTA) curves are given in the Sup-

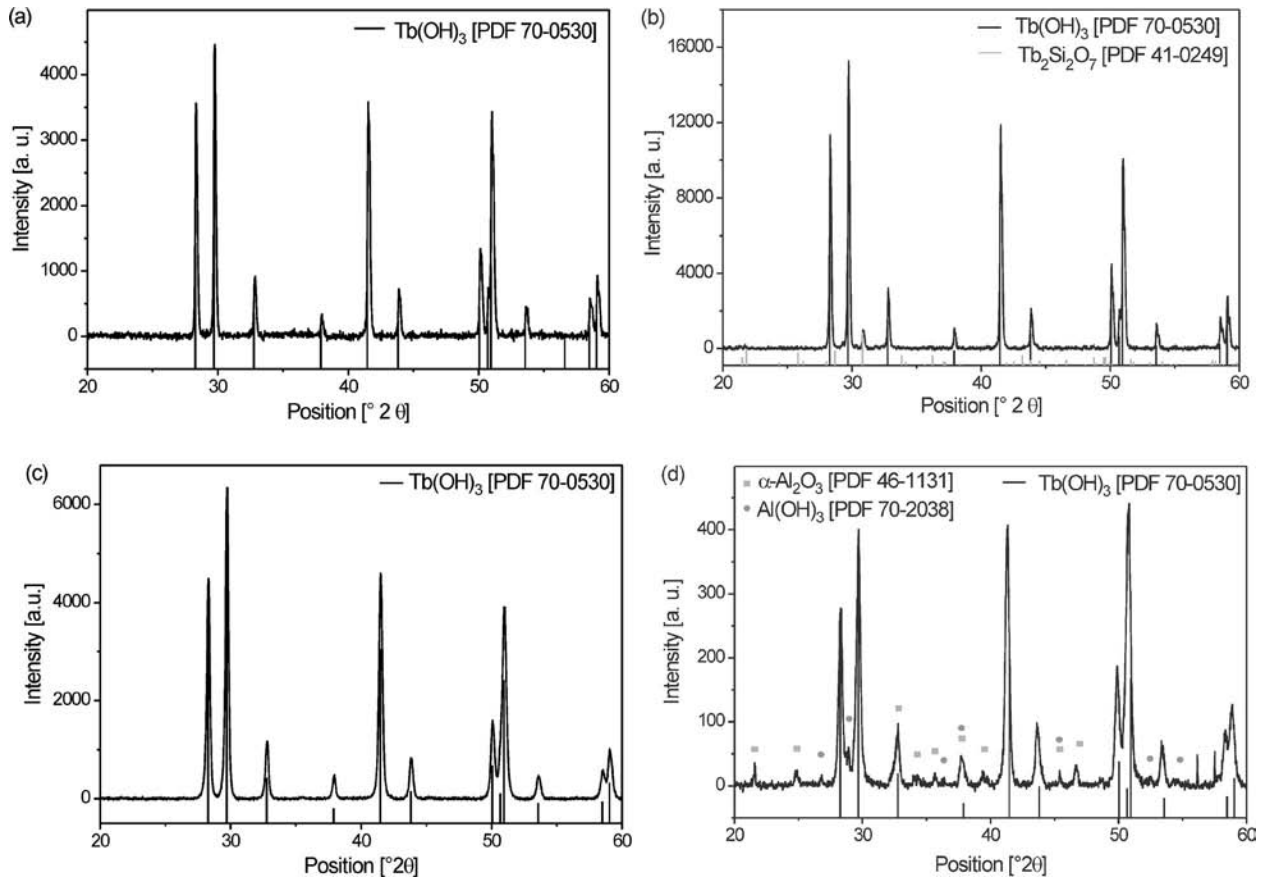

Figure 6. X-ray powder diffraction pattern of powders obtained by solvothermal treatment of the homometallic compounds **1** (a) and **2** (b) and the heterometallic precursors **3** (c) and **4** (d).

porting Information. Solvothermal treatment (250 °C, 24 h) of an 2-propanolic solution of **1** and **2** in an alkaline (aq. KOH, c = 1.87 mol/L) medium produced crystalline terbium hydroxide, $Tb(OH)_3$, as shown by X-ray powder diffraction (Figure 6, a and b).

Powder samples of **2** showed higher crystallinity as evident in the sharpness and intensities of the diffraction peaks. In addition, a crystalline minor phase was also observed, which could be assigned to terbium silicate, $Tb_2Si_2O_7$. The peak at 31° supports the presence of the secondary phase that could result from silicon-containing residual species probably originating from terbium hexamethyldisilylamide or occluded hexamethyldisilazane, which is liberated as a by-product.

The lower crystallinity of powders obtained from **1** can be explained by the different hydrolysis paths of compounds **1** and **2** (Scheme 3). Apparently, the nucleophilic attack (OH^-) in **1** follows a cascade of reactions (hydrolysis + condensation), which is a function of the basicity of the OR groups depending upon their mode of ligation (terminal, doubly- or triply-bridged positions). It can be envisaged that hydrolysis preferentially occurs at the two μ_3-alkoxo groups that cap the Tb_3O_3 plane. As a result, **2** shows a higher number of reaction sites than **1** and is therefore more prone to impurities.

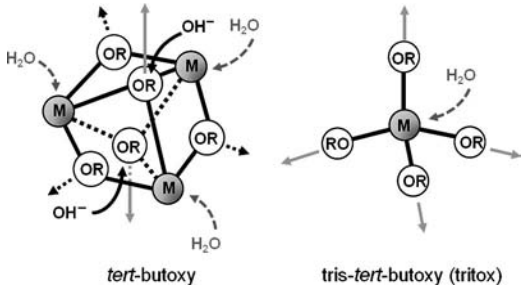

Scheme 3. Possible formation of aqua complexes and condensation directions of intermediate hydroxides produced in the hydrolysis of **1** and **2**.

Transmission electron micrographs (TEM, Figure 7) showed facetted and elongated particles with a rather broad size distribution and a particle size ranging between 70 and 600 nm. The elongated microstructure is apparently favoured by the hexagonal lattice of terbium hydroxide. The lattice fringes (inset in Figure 7, a) seen in high-resolution TEM and the inter planar spacing of 5.8 Å corresponded to the (100) plane of crystalline $Tb(OH)_3$.

The pH of the reaction solution strongly influences the morphology of the $Ln(OH)_3$ structures obtained. Basic conditions, providing a sufficient concentration of OH^-, induce

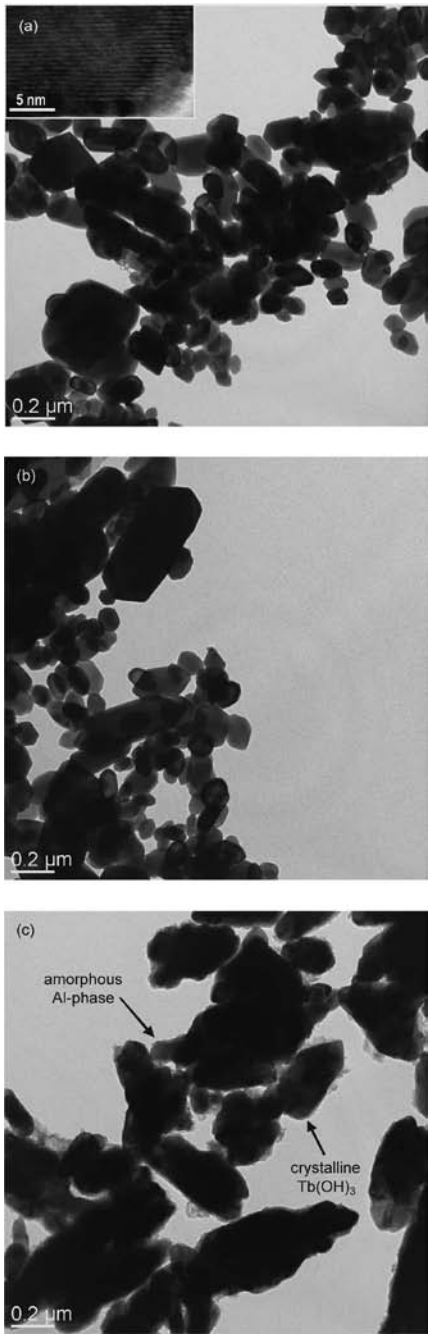

Figure 7. TEM images of powders obtained by solvothermal decomposition of precursors **1** (a), **2** (b) and **3** (c).

the one-dimensional growth of $Ln(OH)_3$ resulting in nanorods or nanowires, whereas a further increase in pH induces the formation of shorter nanorods or plates as observed for $Sm(OH)_3$ and $Gd(OH)_3$ by Li et al.[15a] This phenomenon is the result of a complex interaction between the chemical potential and the ionic motion in the solution.[15a,35] In this case, the hydrolysis is ligand-controlled as the steric profile of the alkoxo ligands limits the number of ligands that can be arranged around the Ln centre; however, there is enough room for the nucleophilic attack by water. The coordinated water molecule is deprotonated on increasing the pH, whereby terminal electronically- and sterically-unsaturated hydroxo groups are formed that bridge other lanthanide centres leading to an assembly of structurally well defined Ln–hydroxo clusters (Scheme 3). Furthermore, the aspect ratio of $Ln(OH)_3$ is not only driven by pH, but is also element specific. Although lighter rare earth hydroxides tend to form elongated structures of high aspect ratio, the heavier rare earth elements, among them Tb, form $Ln(OH)_3$ of lower aspect ratio,[36] which is in agreement with the elongated nanostructures described here (Figure 7).

Solvothermal processing of **3** produced only $Tb(OH)_3$ as the crystalline phase (Figure 6, c), whereas additional peaks were found for **4** (Figure 6, d). As aluminium is present in **3** and **4**, it is evident that the heterometallic frameworks are fragmented under solvothermal conditions causing preferential crystallization of $Tb(OH)_3$ and formation of Al-containing amorphous species [$Al(OH)_3$, AlOOH and Al_2O_3], which require higher temperatures for ordering. The additional peaks in powders produced by **4** can be assigned to transition alumina, δ-Al_2O_3[12b,37] and $Al(OH)_3$, which was confirmed by IR spectroscopy.[38] Discussion of the IR data is provided in the Supporting Information.

The TEM analysis of powders produced by **3** revealed a bimodal morphology distribution in which $Tb(OH)_3$ nanoparticles are surrounded by amorphous aluminium oxide or hydroxide phases (Figure 7, c). The solvothermal treatment of **4** resulted in a resinous solid, which could not be dispersed for TEM sample preparation.

Tb–O–Al Phases by Sol–Gel Processing

We previously reported that sol–gel processing of [NdAl(O*i*Pr)$_6$(*i*PrOH)]$_2$ and [$NdAl_3$(O*i*Pr)$_{12}$(*i*PrOH)] led to monophase $NdAlO_3$ and biphasic oxide–oxide $NdAlO_3/Al_2O_3$ composite, respectively.[29a,29c] However, treatment of the Tb analogues under solvothermal conditions produced only $Tb(OH)_3$ as the crystalline material, which indicates that the hydrolysis kinetics are much faster (than the condensation reaction) under solvothermal conditions, which favours the phase separation into individual terbium and aluminium compounds. Stoichiometric reaction of **3** and **4** with water (3–4 mol-equiv. H_2O per metal centre) produced homogeneous gels, which, upon heat treatment (1000 °C, 2 h), confirmed the formation of terbium aluminate ($TbAlO_3$) as the only crystalline phase in the case of **3** (Figure 8, a), which corresponds to the Tb:Al stoichiometry present in the precursor. In contrast, the heat treated xerogel obtained from **4** revealed AlOOH as the major crystalline phase (Figure 8, b). Additional XRD 2θ values corresponded to the peaks for the garnet ($Tb_3Al_5O_{12}$) and monoclinic terbium aluminate $Tb_4Al_2O_9$ (2θ = 29.2 and 30.5°) phases. This observation shows the influence of the secondary phase on the crystallization and structure of the major phase.[29a,29c] Formation of $Y_4Al_2O_9$ and $YAlO_3$ is reported

as a kinetically stable phase rather than the thermodynamically stable $Y_3Al_5O_{12}$ (YAG) when a mixture of precursors with 3:5 Y:Al ratio was used in spray pyrolysis.[38a,39]

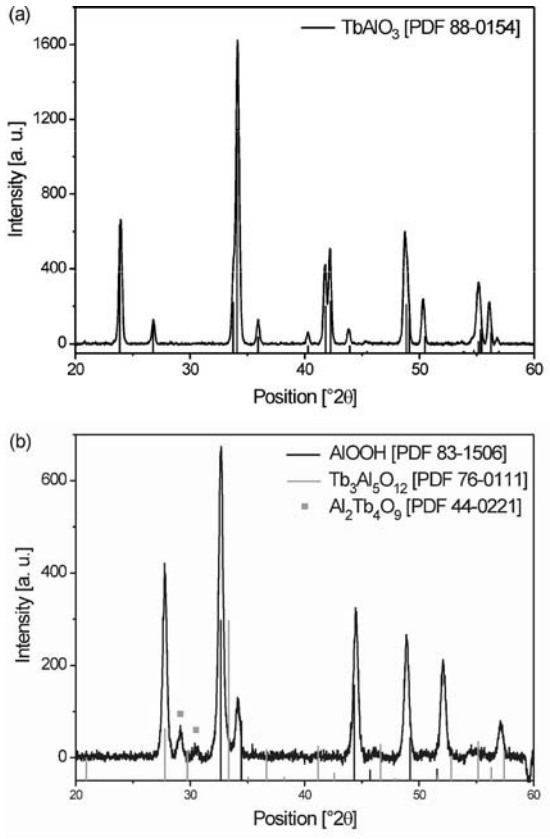

Figure 8. X-ray diffraction pattern of powders obtained by the sol–gel process using heterometallic Tb–Al precursors **3** (a) and **4** (b).

Thin Film Deposition using Compound 4

The heterometallic alkoxide **4** exhibited adequate volatility required for chemical vapour deposition. Analogous lanthanum, neodymium and praseodymium compounds have been used in liquid injection and metal–organic CVD process for the deposition of amorphous $LnAlO_3$ thin films.[12b,27d] We investigated the deposition of thin films using **4** as the precursor on quartz (SiO_2) and spinel ($MgAl_2O_4$) substrates. The as-deposited films were found to be amorphous even at 1000 °C. However, post-thermal treatment at 1350 °C under reduced pressure (p = 10^{-4} mbar, t = 6 h) induced crystallization to produce terbium aluminate in the perovskite phase ($TbAlO_3$) on the quartz substrate (Figure 9, a). Under similar conditions postannealing induced crystallization of $Tb_3Al_5O_{12}$ when $MgAl_2O_4$ was chosen as the substrate (Figure 9, b).

The preferred crystallization of perovskite and garnet phases can be ascribed to the crystallographic relationship between the CVD deposit and substrate materials (Table 5), which showed that the respective lattice mismatches are minimized in the obtained combinations $TbAlO_3$ (a = 5.2296 Å)/SiO_2 (a = 4.9134 Å) and $Tb_3Al_5O_{12}$ (a = 12.000 Å)/$MgAl_2O_4$ (a = 8.0831 Å).

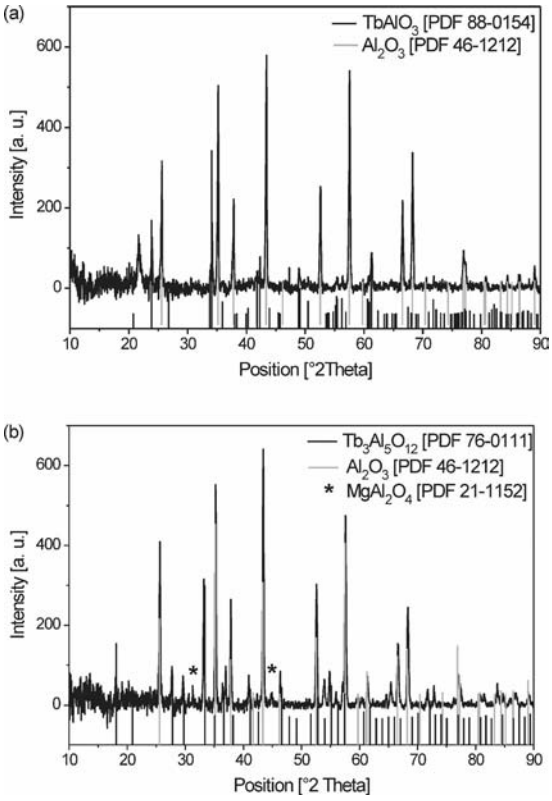

Figure 9. X-ray diffraction patterns of postannealed thin films deposited on a) quartz (SiO_2) and b) $MgAl_2O_4$ substrates using **4** as the precursor.

Table 5. Lattice parameters of the substrate and film materials (PDF [88–0154], [46–1045], [76–0111], [21–1152]).

	Cryst. system	a [Å]	b [Å]	c [Å]	α [°]	β [°]	γ [°]
$TbAlO_3$	orthorhombic	5.2296	5.3058	7.4154	90	90	90
SiO_2	hexagonal	4.9134	4.9134	5.4052	90	90	120
$Tb_3Al_5O_{12}$	cubic	12.000	12.000	12.000	90	90	90
$MgAl_2O_4$	cubic	8.0831	8.0831	8.0831	90	90	90

Optical Properties of the Obtained Powders: Influence of Precursor Chemistry

Emission spectra of the terbium-containing powders obtained from **3** and **4** by sol–gel processing are shown in Figure 10. Both spectra show characteristic peaks corresponding to the 4f→4f transition in Tb^{3+} ions with a maximum peak at 543 nm, which is due to the $^5D_4 \rightarrow {}^7F_5$ transition.[33] Three additional emission bands were observed at 488, 586 and 621 nm, which correspond to the $^5D_4 \rightarrow {}^7F_6$, $^5D_4 \rightarrow {}^7F_4$ and $^5D_4 \rightarrow {}^7F_3$ transitions. Tb^{3+} ions were excited with light in the UV range (λ_{ex} = 277 or 354 nm) which provides enough energy for excitation in the $^5D_3$ energy level and relaxation should result in blue and green emission. However, no emission in the blue range (350–475 nm) was observed, which is ascribed to cross-relaxation processes due to the high concentration of Tb^{3+} in the powders.[40] The spectra obtained for **4** showed better resolution

compared to **3**, which may be due to the higher intensity of the emission from the mixture of terbium aluminates and AlOOH (**4**) allowing detection of the luminescence at a smaller slit width [**3**: λ_{ex} = 354 nm, slit(emission) = 3, slit(excitation) = 3, **4**: λ_{ex} = 277 nm, slit(emission) = 1, slit(excitation) = 2]. Furthermore, taking into account that the green emission is not very sensitive to concentration quenching, the different resolution can be ascribed to the different environment the Tb^{3+} ions are embedded in. The host lattice strongly influences the crystal field resulting in different splittings of the J level. In addition, a lattice without an inversion centre (lower symmetry) means that the parity selection rule can be lifted and higher intensities and better resolutions observed.[41] As described above, X-ray diffraction analysis of the powders obtained from **3** revealed phase-pure $TbAlO_3$ in contrast to a small amount of crystalline $Tb_2Al_4O_9$ and $Tb_3Al_5O_{12}$ in crystalline AlOOH and amorphous aluminium rich phases when **4** was used. This suggests a lower symmetry for **4** explaining the better resolution of the emission spectra obtained.

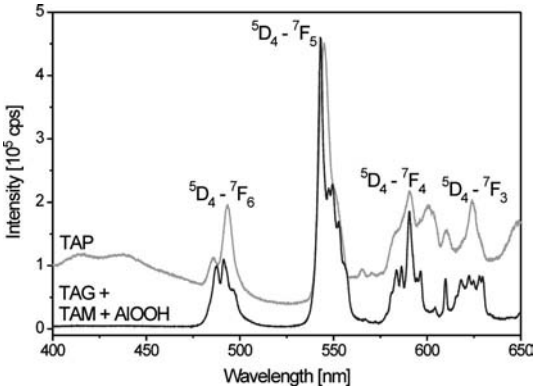

Figure 10. Emission spectra of $TbAlO_3$ (TAP, **3**, λ_{ex} = 354 nm, r.t.) and a mixture of $Tb_2Al_4O_9$ (TAM), $Tb_3Al_5O_{12}$ (TAG) and AlOOH (**4**, λ_{ex} = 277 nm, r.t.) obtained by sol–gel processing.

Conclusions

New terbium-containing homo- and heterometallic alkoxides were synthesized and their molecular structures determined by X-ray diffraction. When used in solvothermal processing terbium *tert*-butoxide (**1**) and terbium tri-*tert*-butoxide (**2**) produced terbium hydroxide. A higher tendency for the formation of a secondary phase was observed for **2**, illustrating the influence of precursor configuration on reactivity and nucleation behaviour due to different hydrolysis and condensation processes. When mixed-metal compounds $[TbAl(OiPr)_6(iPrOH)]_2$ (**3**) and $[TbAl_3(iPrO)_{12}]$ (**4**) were used in solvothermal processing, phase segregation occurred due the instability of the molecular framework producing a mixture of crystalline $Tb(OH)_3$ and amorphous or crystalline aluminium-containing phases [γ-$Al(OH)_3$, δ-Al_2O_3]. In contrast, phase-pure terbium aluminium, $TbAlO_3$, and a mixture of terbium aluminium garnet ($Tb_3Al_5O_{12}$), $Tb_2Al_4O_9$ and AlOOH could be obtained by sol–gel processing of **3** and **4**. The results clearly illustrate the importance of elementary chemical reactions involved in the conversion of a chemical precursor in the solid state, which offers the possibility of imposing a chemical control on the compounds and structures of the final ceramic material. The application of **4** in CVD processing led to thin garnet or perovskite films subject to the nature of the substrate. The optical properties of the obtained terbium aluminate powders were investigated by photoluminescence spectroscopy, which showed the influence of the precursor composition on the optical properties of the resulting materials.

Experimental Section

(I) Precursor Synthesis and Characterization: All manipulations were performed in vacuo and in a nitrogen atmosphere using a modified Schlenk assembly. Solvents used for amide and alkoxide syntheses were purified and dried by standard procedures and stored over sodium or molecular sieves.

$[Tb\{N(SiMe_3)_2\}_3]$: $[Tb\{N(SiMe_3)_2\}_3]$ was synthesized from the reaction between $LiN(SiMe_3)_2$ (60.0 mmol) and $TbCl_3$ [20.0 mmol, Sigma Aldrich, powder, water free, 99.9% dried under dynamic vacuum at 120 °C for at least 1 h and activated by THF (50 mL) at 60 °C for 2 h].[42] $LiN(SiMe_3)_2$ was obtained by the reaction of *n*-butyllithium (477.0 mmol, 300 mL, 1.6 M in hexane, Acros Organics) and hexamethyldisilazane (477.0 mmol, 100 mL, Fluka, > 98.0%) at room temperature for 24 h. The white powder was purified by sublimation at 80 °C before further use.

$[Tb_3(OtBu)_9(HOtBu)_2]$ (1): HO*t*Bu (20 mL) was added to a solution of $[Tb\{N(SiMe_3)_2\}_3]$ (5.7 mmol) in hexane (25 mL) and THF (2 mL) at –195.80 °C. The reaction mixture was stirred at room temperature for 24 h. Condensation and resolution in toluene (15 mL) followed by cooling at –20 °C produced colourless crystals of **1**.

[Tb(tritox)$_3$(THF)] (2): Synthesis of H-tritox (confirmed by NMR) was performed according to a literature procedure.[43] A solution of diethylcarbonate (6.18 mL, Sigma–Aldrich, puriss., >99.5%) in ethyl ether (50 mL) was slowly (2 h) added to a solution of *tert*-butyllithium (90 mL, 1.7 M in pentane, Acros Organics) and stirred at room temperature. For the hydrolysation of residual *tert*-buthyllithium a mixture of water (50 mL) and acetic acid (10 mL) was added (0 °C). The compound was isolated by washing with ethyl ether under addition of sodium hydrogen carbonate. After drying with magnesium sulfate, the product was obtained from the organic phase as a waxy solid that was purified by sublimation at 80 °C.

A solution of H-tritox (4.9 mmol) in hexane (20 mL) was dropped into a solution of $[Tb\{N(SiMe_3)_2\}_3]$ (1.6 mmol) in hexane (50 mL) and stirred at room temperature for 24 h. After condensation the compound obtained was dissolved in a hexane/THF mixture (5 mL/2 mL) and cooled to –20 °C. Colourless crystals were obtained that were identified as $[Tb\{OC(tBu)_3\}_3(THF)]$.

$[TbAl(OiPr)_6(iPrOH)]_2$ (3): A solution of $Al(OiPr)_3$ (6.2 mmol)[44] in benzene (25 mL) was mixed with a solution of **1** (7.8 mmol) in benzene (25 mL). 2-Propanol (20 mL) was added to the mixture, which was stirred at 80 °C for 20 h. After condensation the compound obtained was diluted in toluene and cooled to –20 °C to produce colourless crystals of **3**.

$[TbAl_3(OiPr)_{12}]$ (4): A solution of $Al(OiPr)_3$ (17.3 mmol) in benzene (25 mL) was mixed with a solution of **1** (7.7 mmol) in benzene

(25 mL). 2-Propanol (25 mL) was added to the mixture, which was stirred at 80 °C for 20 h. After condensation of the solvent, resolution in toluene and cooling to –20 °C colourless crystals of **4** were obtained.

Molecular structures of compounds **1**–**4** were determined by X-ray single crystal analysis using a diffractometer AED 2 by Siemens. The molecular structures were solved using SHELXS-86 and SHELXS-93.

CCDC-816882 (for **1**), -817587 (for **2**), -816881 (for **3**), and -816883 (for **4**) contain the supplementary crystallographic data for this paper. These data can be obtained free of charge from The Cambridge Crystallographic Data Centre via www.ccdc.cam.ac.uk/data_request/cif.

Crystal Data for 1: $C_{44}H_{101}O_{11}Tb_3$, M = 1283.01 g/mol, T = 293(2) K, λ = 0.71073 Å, monoclinic, space group $P2(1)/c$, a = 19.625(4) Å, b = 10.831(2) Å, c = 27.509(6) Å, α = 90°, β = 99.39(3)°, γ = 90°, V = 5769(2) Å^3, Z = 4, $\rho_{calcd.}$ = 1.477 Mg/m^3, μ = 3.684 mm^{-1}, $F(000)$ = 2592, 35761 reflections in h(–22/22), k(–12/12), l(–28/29), measured in the range 2.02° ≤ θ ≤ 24.04°, completeness to θ_{max} = 94.5%, 8618 independent reflections, R_{int} = 0.0805, absorption correction: numerical, refinement method: full-matrix least-squares on F^2, data/restraints/parameters: 8618/0/556, $GooF$ = 1.061, $R_{1\ final}$ = 0.0441, $wR_{2\ final}$ = 0.1133, $R_{1\ all}$ = 0.0496, $wR_{2\ all}$ = 0.1198, largest difference peak and hole: 2.253/–2.924 e Å^{-3}.

Crystal Data for 2: $C_{43}H_{89}O_4Tb$, M = 829.06 g/mol, T = 203(2) K, λ = 0.71073 Å, monoclinic, space group P2(1)/n, a = 12.964(3) Å, b = 17.564(4) Å, c = 19.469(4) Å, α = 90°, β = 93.24(3)°, γ = 90°, V = 4425.9(15) Å^3, Z = 4, $\rho_{calcd.}$ = 1.244 Mg/m^3, μ = 1.634 mm^{-1}, $F(000)$ = 1776, 40841 reflections in h(–16/17), k(–22/21), l(–25/25), measured in the range 2.40° ≤ θ ≤ 28.06°, completeness to θ_{max} = 95.8%, 10301 independent reflections, R_{int} = 0.0785, absorption correction: numerical, refinement method: full-matrix least-squares on F^2, data/restraints/parameters: 10301/0/460, $GooF$ = 1.413, $R_{1\ final}$ = 0.0617, $wR_{2\ final}$ = 0.1557, $R_{1\ all}$ = 0.0682, $wR_{2\ all}$ = 0.1590, largest difference peak and hole: 2.080/–1.557 e Å^{-3}.

Crystal Data for 3: $C_{21}H_{50}AlO_7Tb$, M = 600.51 g/mol, T = 293(2) K, λ = 0.71073 Å, triclinic, space group $P\bar{1}$, a = 10.823(2) Å, b = 11.951(2) Å, c = 12.971(3) Å, α = 82.34(3)°, β = 66.74(3)°, γ = 71.23(3)°, V = 1459.4(5) Å^3, Z = 2, $\rho_{calcd.}$ = 1.367 Mg/m^3, μ = 2.484 mm^{-1}, $F(000)$ = 620, 47294 reflections in h(–17/16), k(–20/20), l(–21/22), measured in the range 1.71° ≤ θ ≤ 38.28°, completeness to θ_{max} = 90.3%, 14623 independent reflections, R_{int} = 0.0424, absorption correction: numerical, refinement method: full-matrix least-squares on F^2, data/restraints/parameters: 14623/0/289, $GooF$ = 1.039, $R_{1\ final}$ = 0.0304, $wR_{2\ final}$ = 0.0757, $R_{1\ all}$ = 0.0350, $wR_{2\ all}$ = 0.0800, largest difference peak and hole: 2.385/–3.652 e Å^{-3}.

Crystal Data for 4: $C_{36}H_{84}Al_3O_{12}Tb$, M = 948.89 g/mol, T = 293(2) K, λ = 0.71073 Å, orthorhombic, space group $P2(1)2(1)2(1)$, a = 13.113(3) Å, b = 17.481(4) Å, c = 22.961(5) Å, α = 90°, β = 90°, γ = 90°, V = 5263.5(18) Å^3, Z = 4, $\rho_{calcd.}$ = 1.197 Mg/m^3, μ = 1.440 mm^{-1}, $F(000)$ = 2000, 33013 reflections in h(–15/14), k(–19/19), l(–25/24), measured in the range 2.49° ≤ θ ≤ 24.06°, completeness to θ_{max} = 96.0%, 8003 independent reflections, R_{int} = 0.0333, absorption correction: numerical, refinement method: full-matrix least-squares on F^2, data/restraints/parameters: 8003/0/478, $GooF$ = 1.200, $R_{1\ final}$ = 0.0353, $wR_{2\ final}$ = 0.0920, $R_{1\ all}$ = 0.0376, $wR_{2\ all}$ = 0.0938, largest difference peak and hole: 0.635/–0.769 e Å^{-3}.

(II) Material Synthesis and Characterization: For powder preparation by solvothermal method the precursor (ca. 200 mg) was diluted in 2-propanol (20–25 mL). The solution was activated by addition of aqueous potassium hydroxide solution (1 mL, c = 1.87 mol/L). The activated solution was introduced under ambient conditions in Teflon inliners, which were enclosed in steel autoclaves (DAB-2, Berghof Products + Instruments GmbH) and heated to 250 °C for 24 h. After cooling to room temperature the precipitates were washed several times with methanol and ethanol, collected by centrifugation, dried in air and ground before further characterization.

Sols of the precursors were obtained by solving **3** (1.71 mmol) in a mixture of 2-propanol (100 mL) and toluene (50 mL), and **4** (2.39 mmol) in toluene (100 mL), followed by activation with water (**3**: 0.37 mL H_2O in 20 mL *i*PrOH, T = 80 °C; **4**: 0.56 mL H_2O in 20 mL *i*PrOH, T = 25 °C). The sols obtained were stirred under ambient conditions for several days until the solvent had evaporated. The remains of the solvent were removed from the white xerogels at 160 °C under reduced pressure ($p = 1 \times 10^{-3}$ mbar) for 6 h, followed by calcination.

Thin Tb–O–Al films were deposited on SiO_2 (quartz) and $MgAl_2O_4$ substrates (cleaned by ultra sound in *i*PrOH) with **4**. Precursor flow was set by a precursor temperature of 120–125 °C and a reduced pressure of 10^{-4}–10^{-6} mbar. Substrate temperature was 1000 °C and deposition time was 90 min. The as-deposited films were annealed under reduced pressure ($p = 1 \times 10^{-4}$ mbar) at 1350 °C for 6 h.

Crystallinity and phase of the powders obtained were determined by powder X-ray diffraction at room temperature with a D-5000 by Siemens (40 kV, 25 mA, step width: 0.02°) or a PW 1710 by Philips (45 kV, 30 mA; step width: 0,02°) using Cu-$K_{\alpha 1}$ radiation. X-ray diffraction patterns of the thin films were recorded with a D-5000 by Siemens (40 kV, 25 mA, step width: 0.02°) at room temperature using Cu-$K_{\alpha 1}$ radiation. Phase assignment was affected using the program X'Pert HighScore by Philips Analytical B.V. (Almelo, Netherlands). TEM images were obtained with a transmission electron microscope JEOL 200 CX by Philips. IR spectra were recorded on KBr pellets using a 5 PC FTIR spectrometer by Nicolet. Photoluminescence spectra were obtained with Fluorolog 3–22 spectrometer by Jobin Yvon using a 450-W xenon high-pressure lamp and a photomultiplier R928P for the UV/Vis region.

Supporting Information (see footnote on the first page of this article): TG-DTA data for **1** and **3**, FTIR spectra of powders obtained from **3** and **4** by solvothermal and sol–gel processing.

Acknowledgments

The authors thank the Deutsche Forschungsgemeinschaft (DFG) for financial support (Schwerpunktprogramm SPP1166) and Prof. Kohei Soga for helpful discussions.

[1] D. C. Bradley, H. Chudzynska, M. B. Hursthouse, M. Motevalli, *Polyhedron* **1991**, *10*, 1049–1059.
[2] L. G. Hubert-Pfalzgraf, S. Daniele, A. Bennaceur, J.-C. Daran, M. J. Vaissermann, *Polyhedron* **1997**, *16*, 1223–1234.
[3] a) E. Hemmer, C. Cavelius, V. Huch, S. Mathur, *New Praseodymium Amide and Alkoxide Precursurs for the Synthesis of $Pr(OH)_3$ Nanostructures*, manuscript in preparation; b) E. Hemmer, Y. Kohl, V. Colquhoun, H. Thielecke, K. Soga, S. Mathur, *J. Phys. Chem. B* **2010**, *114*, 4358–4365.
[4] M. Veith, S. Mathur, A. Kareiva, M. Jilavi, M. Zimmer, V. Huch, *J. Mater. Chem.* **1999**, *9*, 3069–3079.
[5] T. J. Boyle, L. J. Tribby, S. D. Bungle, *Eur. J. Inorg. Chem.* **2006**, 4553–4563.
[6] T. J. Boyle, L. A. Ottley, L. N. Brewer, J. Sigman, P. G. Clem, J. J. Richardson, *Eur. J. Inorg. Chem.* **2007**, 3805–3815.

[7] T. J. Boyle, S. D. Bunge, P. G. Clem, J. Richardson, J. T. Dawley, L. A. M. Ottley, M. A. Rodriguez, B. A. Tuttle, G. R. Avilluca, R. G. Tissot, *Inorg. Chem.* **2005**, *44*, 1588–1600.
[8] a) S. Mathur, H. Shen, in: *Encyclopedia of Nanoscience and Nanotechnology* (Ed.: H. S. Nalwa), American Scientific Publishers, **2004**, *4*, p. 131–191; b) T. J. Boyle, L. A. M. Ottley, *Chem. Rev.* **2008**, *108*, 1896–1917; c) A. Pohl, G. Westin, *J. Am. Ceram. Soc.* **2005**, *88*, 2099–2105; d) G. Westin, A. Pohl, M. Ottosson, K. Lashagari, K. Jansson, *J. Sol-Gel Sci. Technol.* **2008**, *48*, 194–202; e) M. Niederberger, G. Gernweitner, J. Buha, J. Polleux, J. Ba, N. Pinna, *J. Sol-Gel Sci. Technol.* **2006**, *40*, 259–266; f) T. J. Boyle, S. D. Bunge, P. G. Clem, J. Richardson, J. T. Dawley, L. A. M. Ottley, M. A. Rodriguez, B. A. Tuttle, G. R. Avilucea, R. G. Tissot, *Inorg. Chem.* **2005**, *44*, 1588–1600.
[9] D. C. Bradley, R. C. Mehrotra, I. P. Rothwell, A. Singh, *Alkoxo and Aryloxo Derivates of Metals*, Academic Press, London, **2001**.
[10] a) F. Meyer, R. Hempelmann, S. Mathur, M. Veith, *J. Mater. Chem.* **1999**, *9*, 1755–1763; b) S. Mathur, M. Veith, T. Ruegamer, E. Hemmer, H. Shen, *Chem. Mater.* **2004**, *16*, 1304–312.
[11] M. Veith, S. Mathur, N. Lecerf, V. Huch, T. Decker, H. P. Beck, W. Eiser, R. Haberkorn, *J. Sol-Gel Sci. Technol.* **2000**, *17*, 145–158.
[12] a) S. Mathur, H. Shen, N. Lecerf, A. Kjekshus, H. Fjellvåg, G. F. Goya, *Adv. Mater.* **2002**, *14*, 1405–1409; b) M. Veith, S. Mathur, H. Shen, N. Lecerf, S. Hüfner, M. H. Jilavi, *Chem. Mater.* **2001**, *13*, 4041–4052.
[13] T. T. Huong, T. K. Anh, L. Q. Minh, *J. Phys: Conference Series* **2009**, *187*, 012064.
[14] C. R. Patra, S. S. A. Moneim, E. Wang, S. Dutta, S. Patra, M. Eshed, P. Mukherjee, A. Gedanken, V. H. Shah, D. Mukhopadhyay, *Toxicol. Appl. Pharmacol.* **2009**, *240*, 88–98.
[15] a) X. Wang, Y. Li, *Angew. Chem. Int. Ed.* **2002**, *41*, 4790–4793; b) N. Zhang, R. Yi, L. Zhou, G. Gao, R. Shi, G. Qiu, X. Liu, *Mater. Chem. Phys.* **2009**, *114*, 160–167.
[16] a) B. L. Cushing, V. L. Kolesnichenko, C. J. O'Connor, *Chem. Rev.* **2004**, *104*, 3839–3946; b) S. Komarneni, *Curr. Sci.* **2003**, *85*, 1730–1734.
[17] G. Wakefield, H. A. Keron, P. J. Dobson, J. L. Hutchison, *J. Phys. Chem. Solids* **1999**, *60*, 503–508.
[18] a) C. Feldmann, *Adv. Funct. Mater.* **2003**, *13*, 101–107; b) K. Riwotzki, H. Meyssamy, H. Schnablegger, A. Kornowski, M. Haase, *Angew. Chem. Int. Ed.* **2001**, *40*, 573–576; c) K. Riwotzki, H. Meyssamy, A. Kornowski, M. Haase, *J. Chem. Phys. B* **2000**, *104*, 2824–2828; d) Y. Gao, C. Shi, Y. Wu, *Mater. Res. Bull.* **1996**, *31*, 439–444.
[19] X. Li, H. Liu, J. Wang, H. Cui, S. Yang, I. R. Boughton, *J. Phys. Chem. Sol.* **2005**, *66*, 201–205.
[20] C. Louis, R. Bazzi, C. A. Marquette, J.-L. Bridot, S. Roux, G. Ledoux, B. Mercier, L. Blum, P. Perriat, O. Tillement, *Chem. Mater.* **2005**, *17*, 1673–1682.
[21] M. Veith, S. Kneip, *J. Mater. Sci. Lett.* **1994**, *13*, 335–337.
[22] J. Gromada, A. Mortreux, T. Chenal, J. W. Ziller, F. Leising, J.-F. Carpentier, *Chem. Eur. J.* **2002**, *8*, 3773–3788.
[23] M. Wedler, J. W. Gilje, U. Pieper, D. Stalke, M. Noltemeyer, F. Edelmann, *Chem. Ber.* **1991**, *124*, 1163–1165.
[24] a) H. A. Stecher, A. Sen, A. L. Rheingold, *Inorg. Chem.* **1989**, *28*, 3282–3283; b) A. Sen, H. A. Stecher, A. L. Rheingold, *Inorg. Chem.* **1992**, *31*, 473–479.
[25] W. A. Herrmann, R. Anwander, M. Kleine, W. Scherer, *Chem. Ber.* **1992**, *125*, 1971–1979.
[26] a) W. A. Herrmann, R. Anwander, F. C. Munck, W. Scherer, V. Dufaud, N. W. Huber, G. R. J. Artus, *Z. Naturforsch. B: Chem. Sci., Teil B* **1994**, *49*, 1789–1797; b) H. A. Stecher, A. Sen, A. L. Rheingold, *Inorg. Chem.* **1988**, *27*, 1132–1133.
[27] a) M. Wijk, R. Norresta, M. Nygren, G. Westin, *Inorg. Chem.* **1996**, *35*, 1077–1079; b) G. Westin, A. Ekstrand, E. Zangellini, L. Börjessin, *J. Phys. Chem. Solids* **2000**, *61*, 67–74; c) G. Westin, M. Moustiakimov, M. Kritikos, *Inorg. Chem.* **2002**, *41*, 3249–3258; d) T. D. Manning, Y. F. Loo, A. C. Jones, H. C. Aspinall, P. R. Chalker, J. F. Bickley, L. M. Smith, G. W. Critchlow, *J. Mater. Chem.* **2005**, *15*, 3384–3387.
[28] R. C. Mehrotra, M. M. Agrawal, *Chem. Commun. (London)* **1968**, 469–470.
[29] a) S. Mathur, M. Veith, H. Shen, S. Hüfner, M. H. Jilavi, *Chem. Mater.* **2002**, *14*, 568–582; b) S. Mathur, M. Veith, R. Rapalaviciute, H. Shen, G. F. Goya, W. L. Martins Filho, T. S. Berquo, *Chem. Mater.* **2004**, *16*, 1906–1913; c) M. Veith, S. Mathur, N. Lecerf, K. Bartz, M. Heintz, V. Huch, *Chem. Mater.* **2000**, *12*, 271–274.
[30] G. R. Giesbrecht, J. C. Gordon, D. L. Clark, B. L. Scott, J. G. Watkin, K. J. Young, *Inorg. Chem.* **2002**, *41*, 6372–6379.
[31] J. Pauls, E. Iravani, P. Köhl, B. Neumüller, *Z. Anorg. Allg. Chem.* **2004**, *630*, 876–884.
[32] a) W. J. Evans, M. A. Ansari, J. W. Ziller, *Polyhedron* **1997**, *16*, 3429–3434; b) P. Biagini, G. Lugli, L. Abis, R. Millini, *J. Organomet. Chem.* **1994**, *474*, C16–C18.
[33] a) D. C. Krupa, D. M. Mahoney, *J. Appl. Phys.* **1972**, *43*, 2314–2320; b) P. Nachimuthu, R. Jagannata, *J. Non-Cryst. Solids* **1995**, *183*, 208–211.
[34] L. Qian, Y. Gui, S. Guo, Q. Gong, X. Qian, *J. Phys. Chem. Solids* **2009**, *70*, 688–693.
[35] Z. A. Peng, X. Peng, *J. Am. Chem. Soc.* **2002**, *124*, 3343–3353.
[36] X. Wang, Y. Li, *Pure Appl. Chem.* **2006**, *78*, 45–64.
[37] a) T. Hinklin, B. Toury, C. Gervais, F. Babonneau, J. J. Gislason, R. W. Morton, R. M. Laine, *Chem. Mater.* **2004**, *16*, 21–30; b) P. Souza Santos, H. Souza Santos, S. P. Toledo, *J. Mater. Res.* **2000**, *3*, 104–114.
[38] a) J. Marchal, T. John, R. Baranwal, T. Hinklin, R. M. Laine, *Chem. Mater.* **2004**, *16*, 822–831; b) T. Hinklin, B. Toury, C. Gervais, F. Babonneau, J. J. Gislason, R. W. Morton, R. M. Laine, *Chem. Mater.* **2004**, *16*, 21–30; c) O. Yamaguchi, K. Takeoka, K. Hirota, H. Takano, A. Hayashida, *J. Mater. Sci.* **1992**, *27*, 1261–1264; d) D. H. Lee, R. A. Condrate Sr., *Mater. Lett.* **1995**, *23*, 241–246.
[39] M. Nyman, J. Caruso, M. J. Hampden-Smith, T. T. Kodas, *J. Am. Ceram. Soc.* **1997**, *80*, 1231–1238.
[40] a) D. J. Robbins, B. Cockayne, B. Lent, J. L. Glasper, *Solid State Commun.* **1976**, *20*, 673–676; b) P. A. M. Berdowski, M. J. J. Lammers, G. Blasse, *Chem. Phys. Lett.* **1985**, *113*, 387–390; c) T. Hayakawa, N. Kamata, K. Yamada, *J. Lumin.* **1996**, *68*, 179–186.
[41] G. Blasse, B. C. Grabmaier, *Luminescent Materials*, Springer, Berlin, Heidelberg, **1994**.
[42] D. C. Bradley, J. S. Ghotra, F. A. Hart, *J. Chem. Soc., Dalton Trans.* **1973**, *10*, 1021–1027.
[43] a) P. D. Bartlett, E. B. Lefferts, *J. Am. Chem. Soc.* **1955**, *77*, 2804–2805; b) P. T. Wolczanski, *Polyhedron* **1995**, *14*, 3335–3362.
[44] D. C. Bradley, R. C. Mehrotra, D. P. Gaur, *Metal Alkoxides*, Academic Press, London, **1978**.

Received: September 9, 2010
Published Online: March 24, 2011

